Progress In Electromagnetics Research M, Vol. 8, 163–180, 2009

MAGNETIO STATIC FIELD ANALYSIS REGARDING THE EFFECTS OF DYNAMIC ECCENTRICITY IN SWITCHED RELUCTANCE MOTOR

H. Torkaman and E. Afjei †

Department of Electrical Engineering
Shahid Beheshti University
Tehran, Iran

Abstract—In this paper, a novel view of a switched reluctance motor under dynamic eccentricity fault to provide the precise and reliable electromagnetics model is presented. It describes the performance characteristics and comparison results of the 6/4 switched reluctance motor with dynamic rotor eccentricity utilizing three-dimensional finite element analysis. The results obtained using three-dimensional finite element analysis of the switched reluctance motor includes flux-linkages, terminal inductance per phase, mutual inductances and static torque for various eccentric motor conditions. In this analysis the end effects and axial fringing fields for simulating reliable model are obtained and presented. The paper continues with comparing these results with the ones obtained for the same motor profile but utilizing two-dimensional finite element method. Finally, Fourier analysis is carried out to study the variations of torque harmonics.

1. INTRODUCTION

Switched reluctance motor (SRM) has many advantages over other types of motors used in a growing number of applications in various industries. The feature's monopoly of SRM such as lack of any coil or permanent magnet on the rotor, simple structure and high reliability, make it a suitable candidate for operation in variable speed, harsh, or sensitive conditions. The different aspects of SRM drives have been

Corresponding author: H. Torkaman (H_Torkaman@sbu.ac.ir).
† H. Torkaman is also with I.A.U, South Tehran Branch, Yang Researchers Club, Tehran, Iran, and Power Electronic and Motor Drives Research Center, Tehran, Iran; E. Afjei is also with Power Electronic and Motor Drives Research Center, Tehran, Iran.

extensively investigated and carried out in the past decades by several research organizations [1].

One of the common faults that can be produced in this motor is eccentricity. Eccentricity exists in a motor when there is an uneven air-gap between the stator and the rotor [2]. If the rotor is eccentric with respect to the shaft, and the bearings are concentric with respect to the stator, then the center of the rotation changes when rotor rotates. This situation is known as the dynamic or rotating eccentricity. Dynamic eccentricity could be the result of a bent shaft and bearing wear. This type of eccentricity occurs when the center of the rotor is not at the center of rotation and the minimum air-gap revolves with the rotor [3].

In [4] the SRM under dynamic and static rotor eccentricity is analyzed using two-dimensional (2-D) finite element method (FEM). It is observed from the results that, with an increase in dynamic eccentricity in the positive direction, the average torque and torque ripple are increased. It is also shown that the average torque change up to 13.2% for motor with 95% dynamic eccentricity. Husain et al. in [5] presented a method for computing the radial magnetic forces in SRM that includes iron saturation and displacement of the rotor from its central location. In this study the unbalanced forces were analyzed using three different methods, namely static two-dimensional FEM, a detailed analytical model, and a simplified analytical model.

The static torque profiles of phases using the two-dimensional FE simulation are obtained in [6] for motor under dynamic eccentricity and it is shown that at low current; the effect of eccentricity is considerable compared to that of the rated current case.

Dorrell et al. in [7] have investigated the effect of eccentricity on torque profile with respect to the switching angle. They have shown that the torque of the motor increases a few percent in fully controlled rated current.

The effect of eccentricity fault on the torque profile of an SRM with 2-D FEM has been investigated in [8] and the result shows that the static torque does not change much with relative eccentricity up to 50%. It is also shown that with an increase in the relative eccentricity, there will be an increase in the fundamental, 8th, 10th, 14th, and 15th torque harmonics. In this study, the results are very much dependent on different motor conditions such as current magnitudes and loads.

It should be mentioned here that in many other researches such as [9–12, 19, 20], the SRM eccentricities have been investigated based on 2-D FEM. It is pointing out that eccentricity fault is considered in the other motors [13, 14] and generators [15].

This paper presents a comprehensive three-dimensional finite element method (3-D FEM) simulation for a 6/4 switched reluctance

motor under dynamic eccentricity rotor as well as eccentricity with a two-dimensional finite element method and then the comparison of the results analyzed.

2. FINITE ELEMENT ANALYSIS

A three dimensional finite element analysis is being used to determine the magnetic field distribution in and around the motor. In order to present the operation of the motor and to determine the static torque at different positions of the rotor, the field solutions are obtained. The field analysis has been performed using a Magnet CAD package [16] which is based on the variational energy minimization technique to determine the magnetic vector potential. The partial differential equation for the magnetic vector potential is [17]:

$$-\frac{\partial}{\partial x}\left(\gamma\frac{\partial \bar{A}}{\partial x}\right)-\frac{\partial}{\partial y}\left(\gamma\frac{\partial \bar{A}}{\partial y}\right)-\frac{\partial}{\partial z}\left(\gamma\frac{\partial \bar{A}}{\partial z}\right)=J \tag{1}$$

where, J is the electric current density (in amper/meter^2); A is magnetic vector potential (in Wb/meter; magnetic flux density is defined as:

$$B=\nabla\times A \tag{2}$$

B is the magnetic flux density (in Tesla or weber/meter^2). Considering appropriate boundary conditions, Eq. (1) is solved to yield the magnetic vector potential.

In the variational method (Ritz method), the solution of Eq. (1) is obtained by minimizing the following functional:

$$F(A)=\frac{1}{2}\iiint_{\Omega}\left[\gamma\left(\frac{\partial A}{\partial x}\right)^2+\gamma\left(\frac{\partial A}{\partial y}\right)^2+\gamma\left(\frac{\partial A}{\partial z}\right)^2\right]d\Omega-\iiint_{\Omega}JAd\Omega \tag{3}$$

which Ω is area under consideration. In the three dimensional finite element analysis, a tetrahedral or hexahedral (rectangular prism) element, with dense meshes at places where the field variations are being changed rapidly has been used.

For the present study, it has been assumed that each stator phase is excited with four-node tetrahedral blocks of current. Also, in this analysis, the usual assumptions such as the magnetic field outside of an air box in which the motor is placed considered to be zero.

The unaligned position is defined when the rotor pole is located across from the stator slot in such a way that the reluctance of the motor magnetic structure is at its maximum. This position is

considered to be at zero degree in the motor performance plot. The aligned position is defined when the rotor pole is fully opposite to the stator pole, in which the reluctance of the motor magnetic structure is at its minimum. This position is assumed to be 44 degrees for the rotor position in the motor performance plots.

In this study, the rotor moves from unaligned to fully aligned position hence, all motor parameters for these points in between can be computed. In order to represent the motor operation and determine the static torque at different rotor positions, the field solutions are obtained at 0, 4, 8, 12, 16, 20, 24, 28, 32, 36, 40 and 44 degrees from the unaligned rotor position. The plots of magnetic flux throughout the motor and parameters have been computed, compared, and elaborated upon.

2.1. The Motor Specifications and Simulation

The motor configuration and specifications used in this study are shown in Table 1 and Figure 1, respectively. The motor phases are clearly marked for later use in Figure 1.

The stator and rotor cores are made up of M-27 non-oriented silicon steel laminations with the following static B-H curve shown in Figure 2 [16].

In this study, each phase winding consists of 120 turns with a current magnitude of 2.5 A. Due to precise comparison between 2-D and 3-D FE analysis, the mesh densities are considered to be exactly the same for both cases. The FE model with mesh densities used in the simulation is as shown in Figure 3.

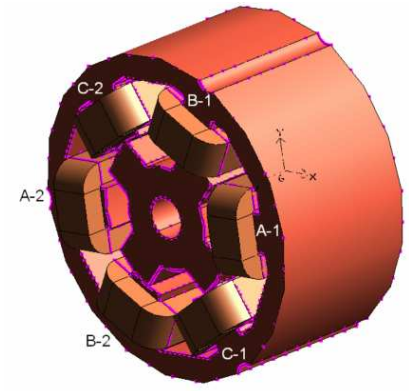

Figure 1. 6/4 SR motor configuration.

Table 1. 6/4 SR motor dimensions.

Parameter	Value
Stator core outer diameter	72 mm
Rotor core outer diameter	40.5 mm
Stack length	36 mm
Length of air gap	0.25 mm
Shaft diameter	10 mm
Rotor pole arc	32°
Stator pole arc	28°
Number of turns	120

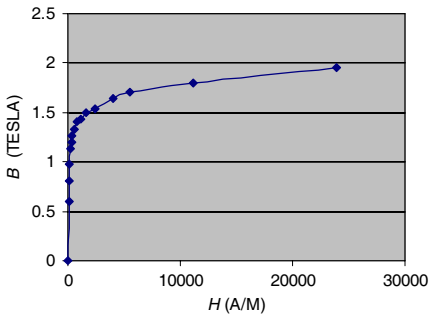

Figure 2. Magnetization curve for M-27 nonoriented silicon steel sheet.

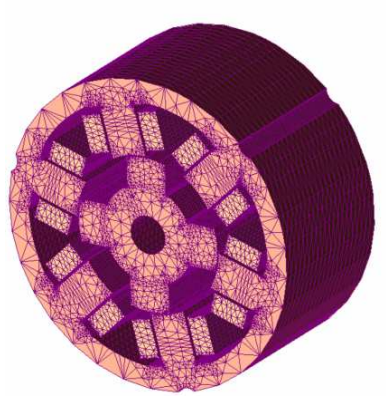

Figure 3. Finite element mesh for the SRM.

2.2. Dynamic Eccentricity

This type of eccentricity occurs when the center of the rotor is not at the center of rotation and the minimum air-gap revolves with the rotor [3]. The non-uniformity of air-gap is time variant when dynamic eccentricity occurs. With respect to the Figure 4 the percentage of dynamic eccentricity is defined as follows:

$$\varepsilon_D = \left(\frac{O_\omega \times O_r}{g} \right) \times 100(\%) \tag{4}$$

where ε_D is the percentage of dynamic eccentricity between the stator and rotor axes; g is the radial air-gap length in the case of uniform

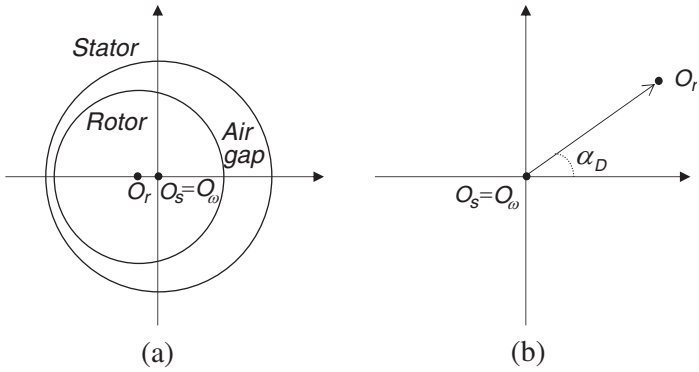

Figure 4. Schematic representation of dynamic eccentricity: (a) Cross-section of stator and rotor positions, (b) dynamic degree definition.

air-gap in healthy motor or with no eccentricity. O_ω, O_r and O_s are the rotor rotation center, rotor symmetry center and stator symmetry center, respectively. In Figure 4(b), α_D shows the initial dynamic eccentricity angle, and $O_\omega \times O_r$ is called the dynamic transfer vector.

Even though manufacturers normally keep the total eccentricity level as low as possible in order to minimize unbalanced magnetic pull (UMP) and to reduce vibration and noise, an air-gap eccentricity of up to 10% is permissible as mentioned in [3, 8, 18]. Due to collision of the rotor pole with stator pole the relative eccentricity of more than 40% is not considered in this study.

3. NUMERICAL RESULTS AND ANALYSIS

To investigate the effects of dynamic eccentricity on the 6/4 switched reluctance behavior, the motor is simulated utilizing 3-D and 2-D finite element analysis.

Flux density shadows and arrows of the healthy motor and the motor with 40% dynamic eccentricity utilizing 3-D FE analysis are shown in Figure 5 and Figure 6, respectively.

In Figure 5 and Figure 6, it is observed that flux density in rotor pole adjacent to the excited stator phase winding has increased with increasing the relative dynamic eccentricity. The reduction of air-gap length and consequently reduction of its related magnetic reluctance causes an increase in the flux density. These unsymmetrical variations in flux densities around the air-gap periphery in turn, result in more noise and vibrations for the motor.

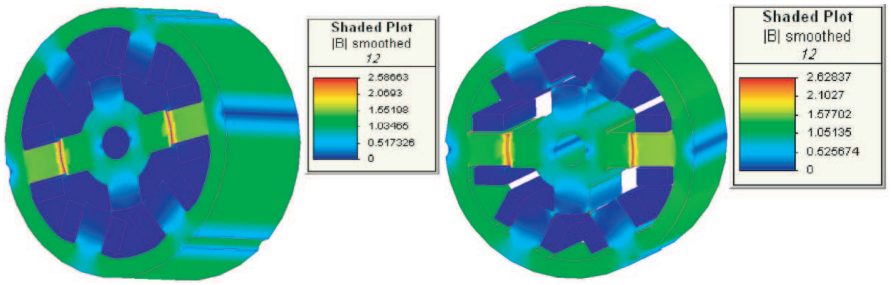

(a) Healthy (b) 40% Eccentricity

Figure 5. Flux density shadow for 3-D FEM: (a) Healthy motor and (b) motor with 40% eccentricity.

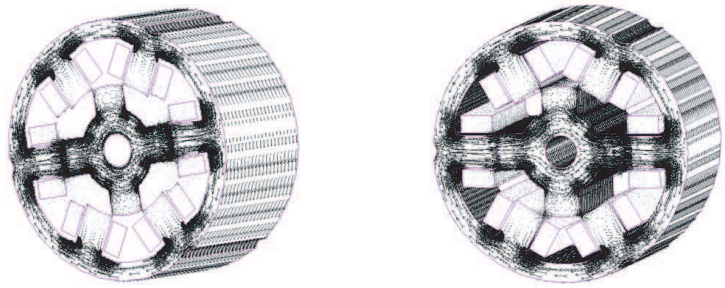

(a) Healthy (b) 40% Eccentricity

Figure 6. Flux density arrows for 3-D FEM: (a) Healthy motor and (b) motor with 40% eccentricity.

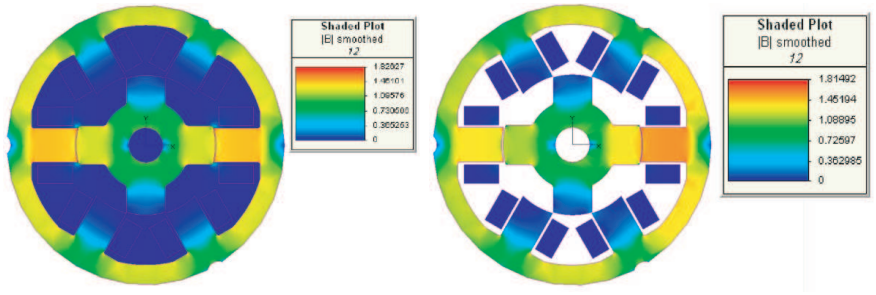

(a) Healthy (b) 40% Eccentricity

Figure 7. Flux density shadow for 2-D FEM: (a) Healthy motor and (b) motor with 40% eccentricity.

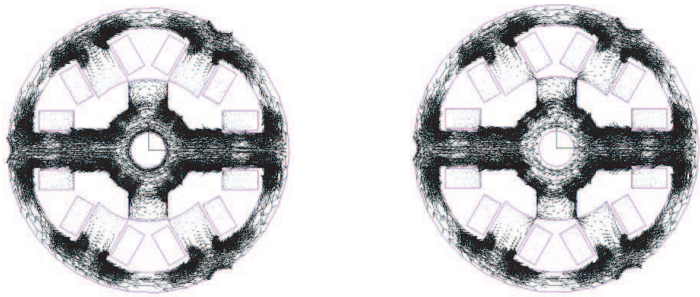

(a) Healthy (b) 40% Eccentricity

Figure 8. Flux density arrows for 2-D FEM: (a) Healthy motor and (b) motor with 40% eccentricity.

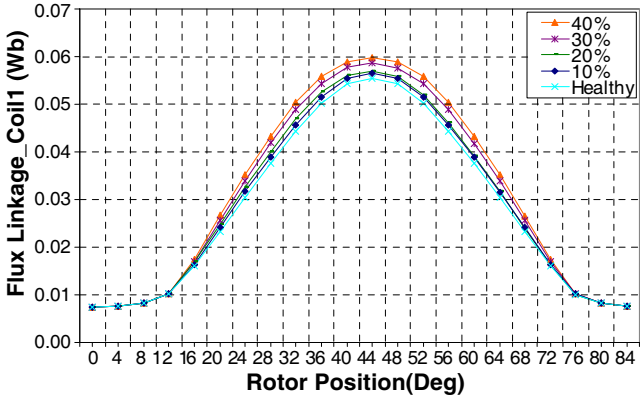

Figure 9. Flux-linkage in A-1 for 3-D FEM.

Flux density shadows and arrows of the healthy motor and the motor with 40% dynamic eccentricity utilizing 2-D FE analysis are shown in Figure 7 and Figure 8 respectively.

As expected, the variations in flux density due to the eccentricity with 3-D FEM are larger than those of the 2-D FEM (Figure 7 and Figure 8), which is due to fringing effect for the field that has been disregarded in 2-D FEM. The variation percentage is defined as follows:

$$Variation = \frac{X_{EM} - X_{HM}}{X_{HM}} \times 100(\%) \tag{5}$$

where, X_{HM}, X_{EM} are any defined parameter values of healthy motor as well as eccentric motor, respectively.

Flux-linkage/rotor position characteristic is one of the most

important profiles of the SRM. Figure 9 shows the flux-linkage of A-1 (coil one in phase A), utilizing 3-D FEM and the variation of rotor position in healthy motor as well as the motor with various dynamic eccentricities.

As shown above the flux linkage peaks at about 44 degrees, correspond to the rotor pole in complete alignment with the related stator pole. Also Figure 9 illustrates that with an increase in the dynamic eccentricity, flux-linkage of coil one of the excited phase (A-1) will increase. It is observed that flux-linkage of the A-1 has 13.3%, 10.3%, 6.6% and 3.6% variations with 40%, 30%, 20% and 10% eccentricity compared with healthy motor, respectively as shown in Figure 10.

The inductance has been defined as the ratio of each phase flux-linkage to the exciting current (λ/I). Since the inductance is directly proportional to the flux linkage, then the resulting inductance values for phase A have 13.3%, 10.3%, 6.6% and 3.6% variations with 40%, 30%, 20% and 10% eccentricity compared with a healthy motor, respectively. This procedure results the same outcomes for other coils in different phases.

Figure 11 shows flux-linkages for A-1 using 2-D FEM with varying rotor positions in healthy motor as well as motor with various dynamic eccentricities in 2-D FEM.

The result of the flux linkages peaks at about 44 degrees, just like the results obtained from the 3-D analysis, but with a maximum of 24% higher values due to the assumption made in 2-D analysis. The 3-D/2-D FEM comparison results of the flux-linkage variations for A-1

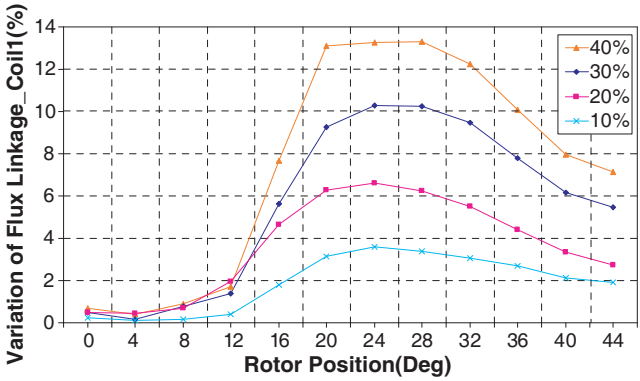

Figure 10. Percentage of variation of flux-linkage in A-1 in eccentric motor to healthy motor for 3-D FEM.

are shown in Figure 12.

The mutual inductance is defined as the ratio of flux-linking that phase to the exciting current in the other phase. According to this definition the mutual inductance values for phases B and C for healthy motor as well as the motor with various eccentricities using 2-D/ 3-D FEM have been calculated and compared.

The variations of mutual inductances for phases B and C using 3-D FEM are presented in Figure 13 and Figure 14, respectively for the motor carrying the rated current of 2.5 A.

Figure 13 shows with an increase in eccentricity, the value of mutual inductance of phase B increases from 44.6% for 10% eccentricity to a maximum of 76.2% for 40% eccentricity. Similarity, Figure 14 illustrates that with increasing eccentricity, the mutual inductance value for phase C will increase from 59% for 10% eccentricity to a peak value of 85.5% for 40% eccentricity. These variations are due to the changes in mutual flux linkages of each coil in that phase.

The static torque developed by the motor is calculated from the ratio of change in the co-energy with respect to the rotor position. The static torque versus rotor position for both healthy motor and with various eccentricities utilizing 3-D FEM is shown in Figure 15.

Due to higher flux linkages in a faulty motor, the static torque obtained is also higher. During the motoring operation (simulated in 3-D FEM) the unbalanced magnetic pull tends to increase the dynamic eccentricity. When 10% eccentricity exists, the motor torque magnitude has up to 4.3% variations (Table 2). Also, this table shows the motor with 20%, 30% and 40% dynamic eccentricities has up to

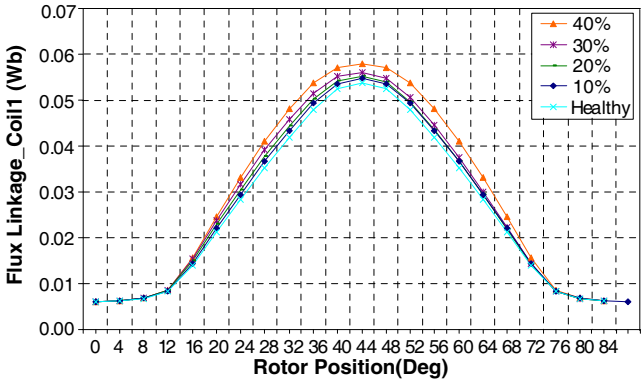

Figure 11. Flux-linkage in A-1 for 2-D FEM.

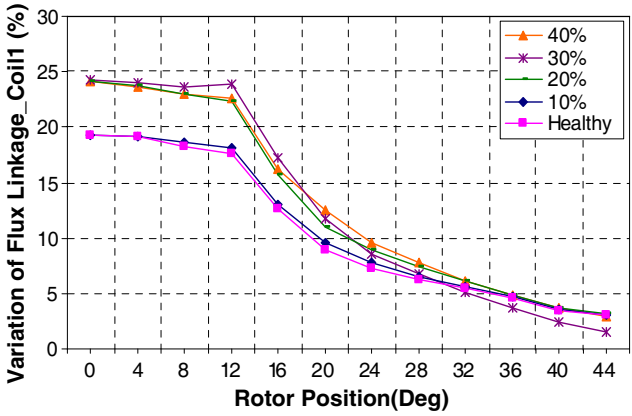

Figure 12. Percentage of variation of flux-linkage in A-1 for 3-D vs. 2-D FEM in healthy motor and motor with various eccentricities.

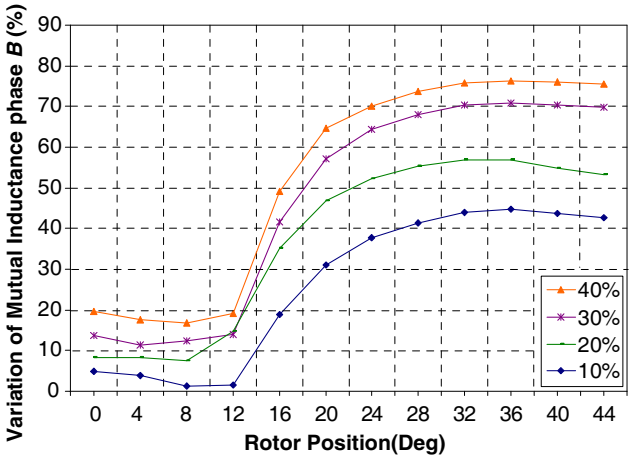

Figure 13. Percentage of variation of mutual inductance in phase B for 3-D FEM for healthy motor vs. motor with various eccentricities.

7%, 8.1% and 13.2% increase in torque variations, respectively.

The static torque versus rotor position for both healthy motor and the motor with various eccentricities utilizing 2-D FEM has been shown in Figure 16.

Due to complete modeling of motor coil windings and also considering the end effects plus axial fringing, the motor simulation in 3-D FEM is more precise and reliable than 2-D FEM simulation.

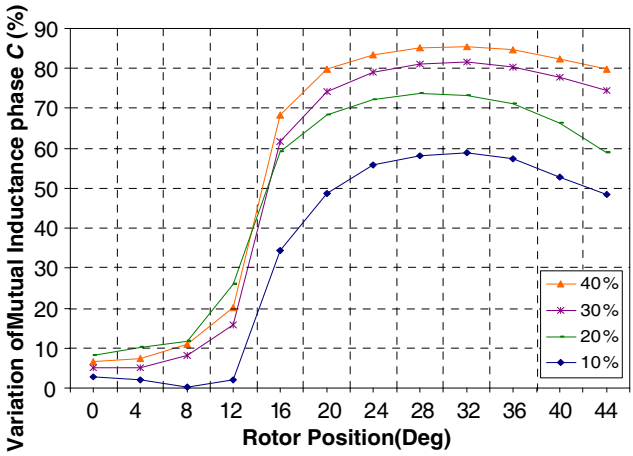

Figure 14. Percentage of variation of mutual inductance in phase C for 3-D FEM for healthy motor vs. motor with various eccentricities.

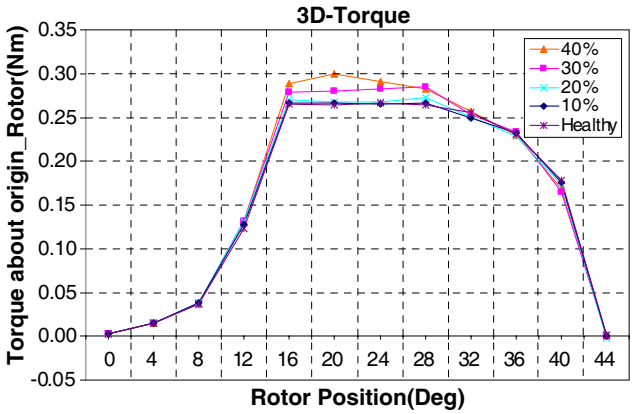

Figure 15. Static torque of the motor vs. rotor position for 3-D FEM: Healthy motor and motor with various dynamic eccentricities.

Table 3 shows the comparison between 3-D and 2-D results for static torque. The average absolute torque is defined in (6).

$$ABS\_Average = \frac{\sum_{i=1}^{n} \left| Eccentricity_i \right|}{n} \tag{6}$$

where n is the number of value and $Eccentricity_i$ is the value of nth eccentricity. According to Eq. (6) and Table 3 the absolute average

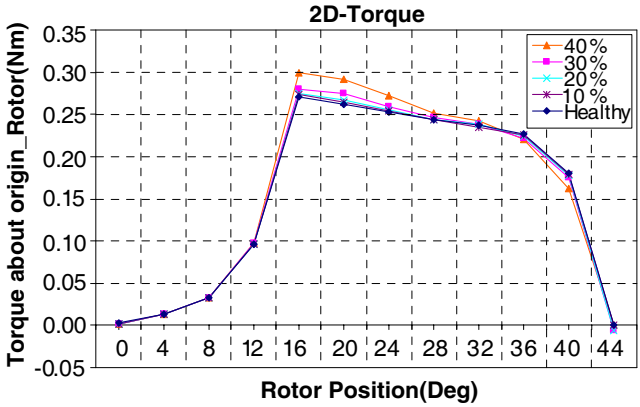

Figure 16. Static torque of the motor vs. rotor position for 2-D FEM: Healthy motor and motor with various dynamic eccentricities.

Table 2. Percentage of variation of torque for 3-D FEM for healthy motor vs. motor with various eccentricities.

Degree	10% Eccentricity	20% Eccentricity	30% Eccentricity	40% Eccentricity
0	−0.64608	−1.04665	−0.60742	−0.65109
4	−0.13025	−0.18173	−1.34245	−0.56049
8	1.30615	1.40194	0.180424	0.032708
12	4.35884	7.0072	6.557116	6.978498
16	0.75793	1.93555	4.854805	8.779511
20	0.51967	1.35769	5.386814	13.28741
24	−0.51106	0.76182	5.820789	9.454833
28	0.71208	3.33119	7.427393	6.742136
32	−2.59001	−1.82419	−0.87997	0.419986
36	0.3212	−1.24276	0.870109	−0.48171
40	−1.43321	−2.87013	−8.18836	−5.0447
44	−1.82347	−2.41758	−3.96404	−3.42164

torque for 3-D FE analysis has 8.5% higher values than the 2-D FE analysis in healthy motor. Also, in eccentric motor with 10%, 20%, 30% and 40% eccentricities, the torque profile produced 9%, 9.5%, 10.4% and 10.5% higher values, respectively.

The non-uniformity of air-gap is time variant when dynamic eccentricity exists; therefore, the distribution of air-gap changes when the rotor rotates. Hence, the torque characteristic of each phase is

Table 3. Percentage of variation of torque for 3-D vs. 2-D FEM in healthy motor and motor with various eccentricities.

Degree	Healthy	10% Eccentricity	20% Eccentricity	30% Eccentricity	40% Eccentricity
0	15.6137	15.1824	14.6759	16.5504	16.6169
4	14.9366	14.7623	14.6412	13.2667	14.2604
8	15.0384	16.4020	16.4257	14.9395	15.0180
12	27.7421	33.4209	36.3618	33.8611	35.3213
16	−2.4411	−2.3006	−1.8818	−0.8054	−4.0177
20	0.7592	0.6204	0.4988	1.5854	2.9633
24	5.2029	4.2096	5.0077	8.8810	6.9941
28	8.4275	9.1670	11.8249	15.8704	11.8684
32	7.7300	5.9925	5.2964	6.2887	6.0293
36	2.0968	2.6553	1.6861	4.9914	4.3221
40	−1.1496	−1.9901	−3.1620	−5.9501	3.9208
44	−1.7900	−2.4000	−2.6000	−2.8000	4.8000

changed in different rotor positions and repeated identically after one complete revolution.

3.1. Fourier Analysis of Torque/Rotor Angular Position Characteristic

Results of harmonic components analysis of the static torque profiles for 3-D FEM for various eccentricities are presented in Figure 17 using MATLAB software. With the increase in the dynamic eccentricity there is an increase in the fundamental harmonic torque. Fundamental harmonic torque in 3-D FEM has higher value than 2-D FEM.

Table 4 shows the variation of the fundamental, 3rd, 5th, and 7th harmonic torques for healthy motor and motor with dynamic eccentricity for 3-D versus 2-D FE analysis. It is observed that the 3rd, 5th, and 7th harmonic torques for 3-D FE analysis has 12.1%, 21.8% and 60.3% lower values than the 2-D FE analysis in healthy motor, respectively. Also, in eccentric motor with various eccentricities, the 3rd, 5th, and 7th harmonic torques produced 16%, 6.9% and 47.3% lower values in peak, respectively.

Table 4. Percentage of variation of harmonic torque for 3-D vs. 2-D FEM in healthy motor and motor with various eccentricities.

Harmonic Component	Healthy	10% Eccentricity	20% Eccentricity	30% Eccentricity	40% Eccentricity
Fundamental	4.34805	4.620625	5.244103	6.933711	6.228796
3rd	−12.1291	−6.15648	−8.80069	−16.0505	−10.8286
5th	−21.8723	−6.93132	−4.97512	−5.75949	−6.98138
7th	−60.3604	−32.8302	−38.5805	−47.3458	−37.037

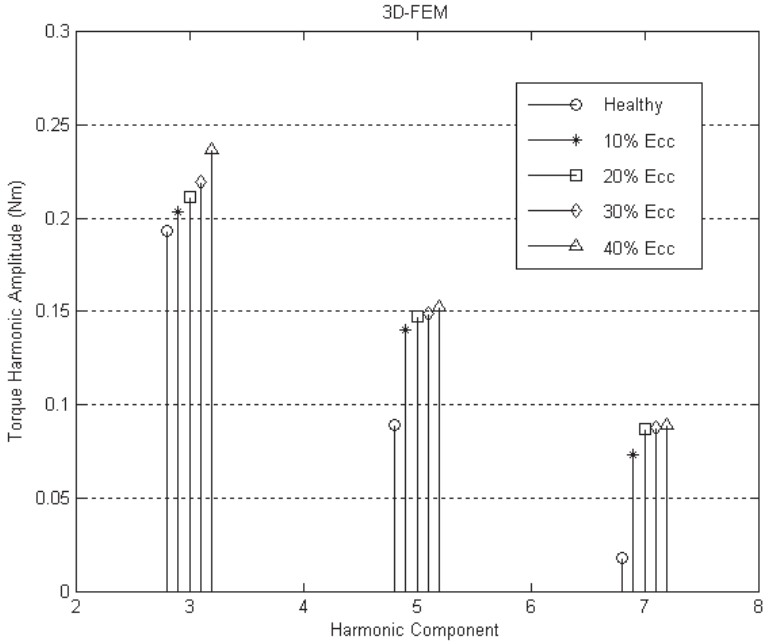

Figure 17. Torque harmonic amplitude for 3-D FEM in healthy motor and motor with various eccentricities.

4. CONCLUSION

Finite element method is a valuable tool for magnetic design and performance calculations of switched reluctance motor parameters.

This study can be accounted for as a comprehensive study of dynamic rotor eccentricity analysis by 3-Dimensional as well as 2-D finite element method in switched reluctance motor.

In this paper, the effects of dynamic eccentricity on flux density, flux-linkage, terminal inductance, mutual inductance, and torque profile in switched reluctance motor with 3-D FEM were analyzed. Then the results were compared with those obtained from 2-D FEM.

The different values of flux densities obtained in excited stator poles and the corresponding rotor poles under dynamic eccentricity show more radial forces hence result in more noise and vibration. The computed results show that motor with 10%, 20%, 30% and 40% dynamic eccentricity has 4.3%, 7%, 8.1% and 13.2% increase in torque profile. The average absolute torque for 3-D FE analysis has 8.5% higher value than 2-D FE analysis in healthy motor. In 2-D FE analysis, the torque values obtained for eccentric motor with 10%, 20%, 30% and 40% eccentricity are 9%, 9.5%, 10.4% and 10.5% higher, respectively. The variations between 2-D/3-D FE results are due to consideration of the end effects and also axial fringing field in 3-D FE analysis.

This analysis shows that with increasing dynamic eccentricity, the values of the flux density, flux-linkage, mutual inductance, terminal inductance and torque are increased.

REFERENCES

1. Torkaman, H. and E. Afjei, "Comprehensive study of 2-D and 3-D finite element analysis of a switched reluctance motor," *Journal of Applied Sciences*, Vol. 8, No. 15, 2758–2763, 2008.
2. Torkaman, H. and E. Afjei, "Comprehensive magnetic field-based study on effects of static rotor eccentricity in switched reluctance motor parameters utilizing three-dimensional finite element," *Electromagnetics*, Vol. 29, No. 5, 421–433, Taylor and Francis, 2009.
3. Guldemir, H., "Detection of airgap eccentricity using line current spectrum of induction motors," *Electric Power Systems Research*, Vol. 64, No. 2, 109–117, Elsevier, 2003.
4. Sheth, N. K. and K. R. Rajagopal, "Variations in overall developed torque of a switched reluctance motor with air-gap nonuniformity," *IEEE Transactions on Magnetics*, Vol. 41, No. 10, 3973–3975, Oct. 2005.
5. Husain, I., A. Radun, and J. Nairus, "Unbalanced force calculation in switched-reluctance machines," *IEEE Transaction on Magnetics*, Vol. 36, No. 1, 330–338, Jan. 2000.
6. Faiz, J. and S. Pakdelian, "Finite element analysis of switched reluctance motor under dynamic eccentricity fault," *12th*

International Power Electronics and Motion Control Conference, 1042–1046, Aug. 2006.

7. Dorrell, D. G., I. Chindurza, and C. Cossar, "Effects of rotor eccentricity on torque in switched reluctance machines," *IEEE Transaction on Magnetics*, Vol. 41, No. 10, 3961–3963, Oct. 2005.
8. Sheth, N. K. and K. R. Rajagopal, "Effects of nonuniform air-gap on the torque characteristics of a switched reluctance motor," *IEEE Transactions on Magnetics*, Vol. 40, No. 4, 2032–2034, Jul. 2004.
9. Geldhof, K. R., T. J. Vyncke, F. M. L. L. De Belie, L. Vandevelde, J. A. A. Melkebeek, and R. K. Boel, "Embedded runge-kutta methods for the integration of a current control loop in an SRM dynamic finite element model," *IET Science. Meas. Technology.*, 17–20, 2007.
10. Parreira, B., S. Rafael, A. J. Pires, and P. J. Costa Branco, "Obtaining the magnetic characteristics of an 8/6 switched reluctance machine: From FEM analysis to the experimental tests," *IEEE Transactions on Industrial Electronics*, Vol. 52, No. 6, 1635–1643, Dec. 2005.
11. Kamper, M. J., S. W. Rasmeni, and R.-J. Wang, "Finite-element Time-step simulation of the switched reluctance machine drive under single pulse mode operation," *IEEE Transaction on Magnetics*, Vol. 43, No. 7, 3202–3208, Jul. 2007.
12. Sixdenier, F., L. Morel, and J. P. Masson, "Introducing dynamic behaviour of magnetic materials into a model of a switched reluctance motor drive," *IEEE Transaction on Magnetics*, Vol. 42, No. 3, 398–404, Mar. 2006.
13. Faiz, J. and B. M. Ebrahimi, "Mixed fault diagnosis in three-phase squirrel-cage induction motor using analysis of air-gap magnetic field," *Progress In Electromagnetics Research*, PIER 64, 239–255, 2006.
14. Faiz, J., B. M. Ebrahimi, and M. B. B. Sharifian, "Time stepping finite element analysis of broken bars fault in a three-phase squirrel-cage induction motor," *Progress In Electromagnetics Research*, PIER 68, 53–70, 2007.
15. Faiz, J., B. M. Ebrahimi, M. Valavi, and H. A. Toliyat, "Mixed eccentricity fault diagnosis in salient-pole synchronous generator using modified winding function method," *Progress In Electromagnetics Research B*, Vol. 11, 155–172, 2009.
16. Magnet CAD package: User Manual, Infolytica Corporation Ltd., Montreal, Canada, Jan. 2007.

17. Afjei, E., A. Sydatan, and H. Torkaman, "A new two phase bidirectional hybrid switched reluctance motor/field-assisted generator," *Journal of Applied Science*, Vol. 9, No. 4, 765–770, 2009.
18. Nandi, S., H. A. Toliyat, and X.-D. Li, "Condition monitoring and fault diagnosis of electrical motors — A review," *IEEE Transactions on Energy Conversion*, Vol. 20, No. 4, 719–729, Dec. 2005.
19. Li, J., D. Choi, and Y. Cho, "Analysis of rotor eccentricity in switched reluctance motor with parallel winding using FEM," *IEEE Transactions on Magnetics*, Vol. 45, No. 6, 2851–2854, 2009.
20. Dorrell, D. G. and C. Cossar, "A vibration-based condition monitoring system for switched reluctance machine rotor eccentricity detection," *IEEE Transactions on Magnetics*, Vol. 44, No. 9, 2204–2214, 2008.